ACS APPLIED MATERIALS & INTERFACES

Letter

www.acsami.org

Hybrids of carbon Nanotube Forests and Gold Nanoparticles for Improved Surface Plasmon Manipulation

Taron Makaryan,*[,†,‡] Santiago Esconjauregui,[†] Manuel Gonçalves,[§] Junwei Yang,[†] Hisashi Sugime,[†] Dirk Nille,[§] Pathabi Raman Renganathan,[§] Pola Goldberg-Oppenheimer,[†,⊥] and John Robertson[†]

[†]Department of Engineering, University of Cambridge, Cambridge CB3 0FA, United Kingdom

[‡]Faculty of Radiophysics, Yerevan State University, Yerevan 0005, Armenia

[§]Institute of Experimental Physics, Ulm University, Ulm 89069, Germany

[⊥]School of Chemical Engineering, University of Birmingham, Edgbaston B15 2TT, United Kingdom

ABSTRACT: We report the fabrication and characterization of hybrids of vertically-aligned carbon nanotube forests and gold nanoparticles for improved manipulation of their plasmonic properties. Raman spectroscopy of nanotube forests performed at the separation area of nanotube-nanoparticles shows a scattering enhancement factor of the order of 1×10^6. The enhancement is related to the plasmonic coupling of the nanoparticles and is potentially applicable in high-resolution scanning near-field optical microscopy, plasmonics, and photovoltaics.

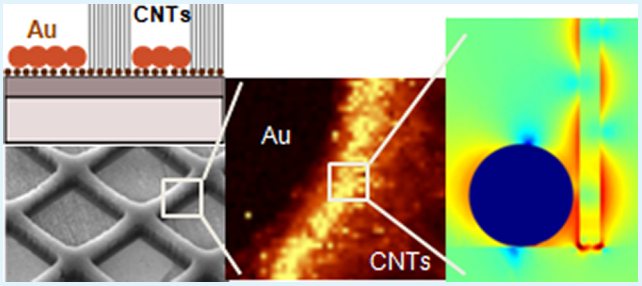

KEYWORDS: *SERS, carbon nanotubes, gold nanoparticles, hybrid nanostructure*

INTRODUCTION

Surface-enhanced Raman scattering (SERS) utilizes plasmonic properties of noble metal nanoparticles (MNPs) in order to detect scattered light modulated by atomic vibrations within the nanoparticles.[1,2] This is performed at certain focused light areas ("hot spots") generated either at the MNP surface because of its roughness or at nanoscale interparticle spaces.[3] Fabrication of MNP-based structures which provide cost-effective, multiple route access for such characterizations and applications still remains a challenge. This problem can be addressed by incorporating another source of surface plasmons (SPs) with those of noble metals, thus increasing the detected signal intensity.

Carbon nanotubes (CNTs) and graphene have been suggested as potential SP enhancers.[4−7] Graphene can be grown only on a few specific metallic substrates and then transferred by wet chemical method onto a plasmonic device.5 This however has the drawback of being spatially non-selective at the microscale level and non scalable. CNT forests (i.e. nanotubes vertically self-aligned to a substrate during the growth), in contrast, can be fabricated on a wider variety of substrates, on patterned geometries,[8] and with control over nanotube length.[9,10] Therefore, the requirements for intensive light scattering properties and fabrication reproducibility urge the choice of CNT forests as plasmonic components. Recently, the plasmonic properties of CNTs have been studied on individual tubes decorated by Au nanoparticles,[11−13] horizontal networks of CNTs on an Au surface,[14,15] or on nanotube forests covered by Au nanoparticles.[16−18] All these studies, however, have overlooked the possibility of the enhancement of plasmonic properties of the forests grown near noble MNPs.

Herein, we study this concept by fabricating CNT forest-Au nanoparticle hybrid arrays and investigating the mediated amplification of Raman signal intensity from CNTs by Au nanoparticles SPs, as schematically depicted in Figure 1.

For demonstrating the SERS detection, we use benzenethiol (BT) and methylene blue (MB) deposited onto the samples. We find a SERS signal enhancement factor $\geq 1 \times 10^6$ at the separation area of CNT forest and Au nanoparticles. The Raman increase is also confirmed by finite element method (FEM) numerical simulations. Using FEM, we study the electric field distribution and enhancement on a system consisting of a CNT and Au nanoparticle supported by a silica substrate. The diameter and length of CNTs, which can be tuned in their growth process, play a crucial role. We have noticed that long CNT forests screen the Raman signal from the Au nanoparticles showing no Raman enhancement increase at the Au nanoparticles-nanotube forest separation area. We have therefore grown CNT forests of ~500 nm in height to obtain SERS improvement at the separation area of the nanomaterials. The advantages of the fabricated structure are the strong electromagnetic interaction of nanoparticles, their fabrication reproducibility, and the separation area of CNTs and MNPs.

Received: September 30, 2013
Accepted: April 11, 2014
Published: April 11, 2014

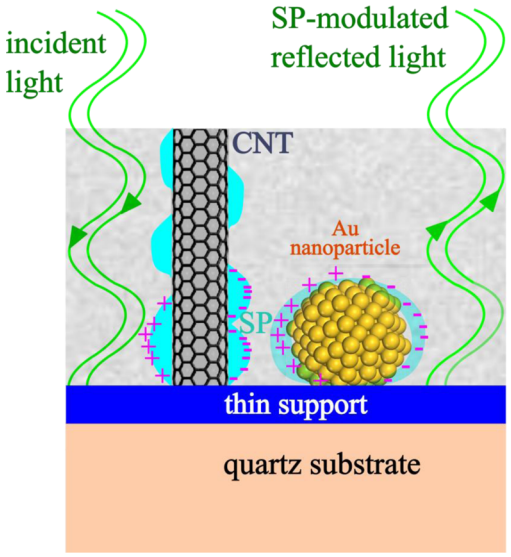

Figure 1. Schematic of the enhancement effect of Raman signal of Au nanoparticles by the surface plasmons of a metallic CNT, deposited on top of Al support on a silica substrate. The localized SPs of the Au nanoparticle couple to the SPs of CNTs.

EXPERIMENTAL SECTION

We grow patterned CNT forests at the vicinity of the as-deposited Au nanoparticles, as shown in Figure 2. For that, we first evaporate a film of 10 nm Al on a silica substrate ($\sim 1 \times 10^{-6}$ mbar base pressure) and subsequently (via air transfer) 1 nm high-purity Fe (Figure 2a). The actual Fe support is Al_2O_3. Thereafter, we pattern a film of 30 nm Au ($\sim 1 \times 10^{-6}$ mbar base pressure evaporation) through a shadow mask, Figure 2b. The shadow mask consists of open squares of 70×70 μm^2 (through which Au is deposited) defined by perpendicularly crossing 30 μm wide lines. The inset of Figure 2b shows an atomic force microscopy (AFM) image of Au after deposition. After metal evaporations, we place the samples in a hot-wall furnace tube for catalyst pretreatment and nanotube growth. We use purely chemical vapor deposition (CVD). We evaluate different CNT growth conditions for this particular catalyst.9 For catalyst pre-treatment, we heat up the samples from room temperature (RT) up to 680 °C in total 1 bar pressure of Ar:H_2 = 400:600 sccm gas flow at a ramping rate of 60° C min^{-1}. Upon reaching the growth temperature, we switch the gas flow to 600 sccm Ar and 2000 sccm H_2. Immediately afterwards, we add 5 sccm C_2H_2 to the system for CNT growth and maintain for 3.5 min. We thus obtain ~500 nm thick forests (inset of Figure 3e). Finally, we cool the samples with 4000 sccm Ar flow and remove from the furnace at RT.

The effect of CVD annealing on the morphology of Au nanoparticles is analyzed by AFM, insets of Figure 2b, c. The plot in Figure 2b compares the profiles heights of Au nanoparticles at the border with the CNT forest, before (blue line, Figure 2b inset) and after (black line, Figure 2c inset) CVD annealing. The root-mean-square roughness of the as-annealed Au nanoparticles (~1.85) is calculated to be 43% more than that of the as-deposited MNPs (~1.58). The area density of the CNTs is determined by the active catalyst nanoparticles on the Al_2O_3 template. To get the maximum coupling of the Au nanoparticles to the CNTs, these can be engineered by adjusting the Au and catalyst nanoparticles deposition thickness, annealing, and CNT growth temperature in the CVD system.[10]

Scanning electron microscopy (SEM) analysis shows forest growth near the patterned Au nanoparticles, Figure 2c. The forests grow in the areas (indicated in Figure 2c), which are covered by the crossing lines of the mask during the Au evaporation thus creating hybrid nanostructures consisting of CNT forests and Au nanoparticles. After growth, we evaporate nominal 3 nm Au onto the samples (Figure 2d) without any mask, in order to cover the CNTs with MNPs providing more hot spots for SERS measurements. For BT deposition, we dip the substrates into a 10 mM BT solution for 2 h, and then blow dry with N_2. For MB deposition, we drop cast the substrate with a 1 μM MB ethanol solution and leave it to dry in ambient. We then wash away the excess MB molecules using triple deionized water and subsequently iso-propanol. High-resolution transmission electron microscopy analysis of the tubes reveals triple-walled CNTs with an average diameter of 7 nm (not shown here). We perform Raman spectroscopy mapping along the border of CNT forests and Au nanoparticle islands, acquiring for 0.5 s by 632 nm wavelength He−Ne laser 0.25 mW excitation with a 0.95 numerical aperture and a 100× magnification objective.

RESULTS AND DISCUSSION

The forests are evaluated for vertical waveguides of SPs by Raman spectroscopy as shown in Figure 3. The SEM image of Figure 3a details an area of the patterned hybrid Au-CNT-Au nanostructure. The confocal optical image of Figure 3b displays the border of the Au island-CNT forest hybrid nanostructure where Raman mapping reveals increased signal enhancement. The Raman mapping image (Figure 3c) shows the signal intensity of the Au-CNT-Au nanostructure in the wavelength range from 1250 to 1700 cm^{-1}.

If Au nanoparticles are placed adjacent to the CNTs, the SPs of both nanomaterials couple, as previously suggested.[19] Therefore, the excited SPs on the root of the CNTs can propagate up to the tip. Due to this optical coupling, the CNT forests at the border of the Au nanoparticle islands are seen bright yellow in Figure 3c, and those far from the edge are seen brownish. We present reference Raman measurements results (Figure 3d) after each step of the sample preparation in order to assess the contribution of each component independently. Namely, typical Raman spectra from pristine Au islands (curve 1), pristine CNT forests of the Au-CNT hybrid nanostructure (curve 2), CNT forests covered by 3 nm Au at spots far from (curve 3, yellow circle in Figure 3c) and adjacent to (curve 4, red circle in Figure 3c) the Au islands are presented in Figure 3d. The resulting Raman enhancement can be calculated by the method described previously.[17] Briefly, it is done by using the fact that Raman signal is collected from the focused area of the incident laser spot, whereas the plasmonic signal is concentrated at a much smaller hot spot. By taking this focused area as the diffraction limited laser spot size, we calculate the Raman enhancement of the Au-CNT-Au nanostructure at the separation area (curve 4) from Figure 3d to be 6.2×10^5 (CNT D-peak at wavenumber 1606 cm^{-1}). Farther from the separation area, this value is 4.7×10^5 (same D-peak wavenumber) as can be seen from the inset of Figure 3d (curve 3). This Raman enhancement ~30% increase along the separation area of CNT-Au nanoparticles confirms their optical coupling. The additional Au deposition decreases the CNT Raman D/G peak ratio from 0.991 to 0.965, as seen from the

dx.doi.org/10.1021/am501863g | ACS Appl. Mater. Interfaces 2014, 6, 5344−5349

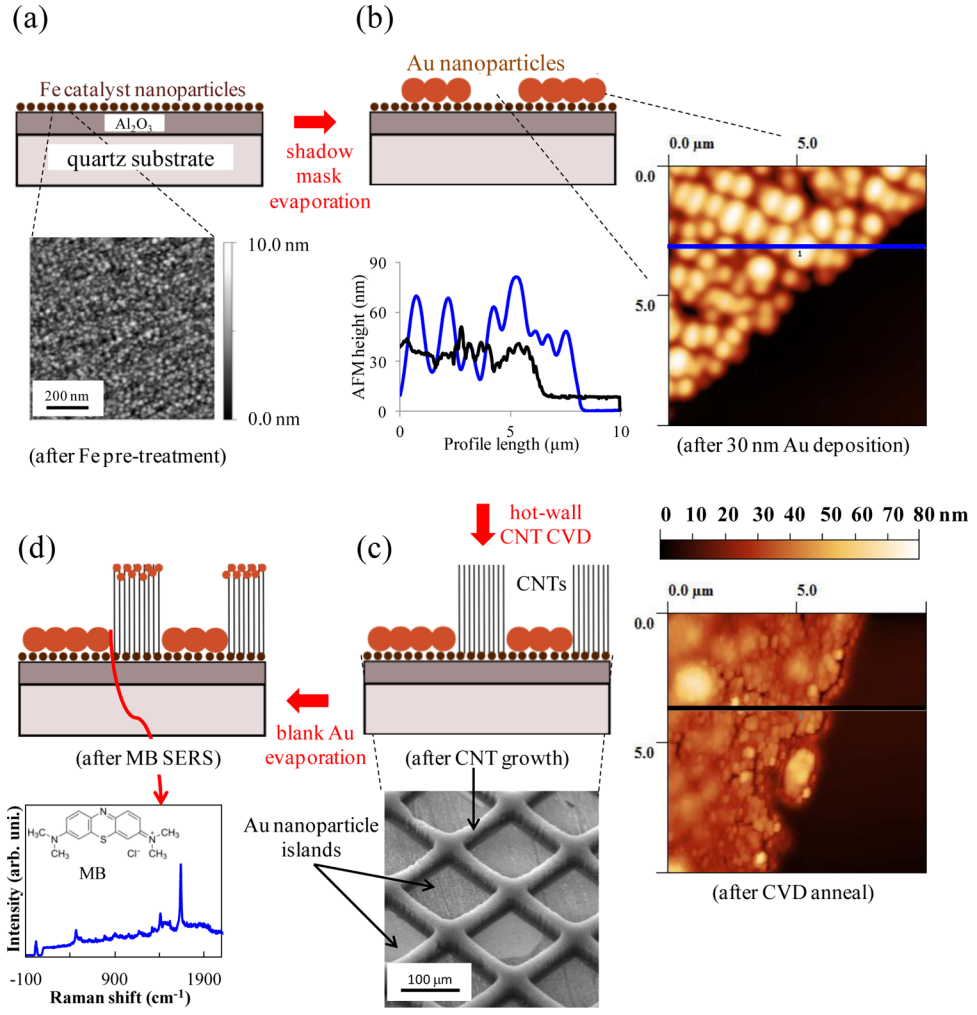

Figure 2. Schematics of the hybrid nanostructure fabrication processes: (a) blank Fe and Al and (b) shadowed Au thermal evaporation steps are followed by (c) a CVD process for growing CNTs in the area between Au nanoparticle islands, and (d) an additional deposition of small Au nanoparticles on top of CNTs for SERS. Inset in a shows AFM image of Fe nanoparticles deposited on alumina. AFM images in the insets of b and c show the Au nanoparticles before and after CVD run, the corresponding blue and black lined profiles of which are compared in the inset graph of b. SEM image of the inset in c shows the CNT forest grown near the patterned Au nanoparticle islands. The inset of d is a SERS spectrum after blank evaporation of 3 nm Au and MB deposition at the separation area of CNT forest-Au nanoparticle island of such a pattern unit.

Gaussian fitting of the curves 3 and 4, Figure 3d (inset). This ~3% change of the CNTs D-peak rules out the possibility of introducing significant defects by 3 nm Au deposition.

Furthermore, for evaluating sensing properties of the proposed hybrid nanostructure, SERS factor of BT (Figure 3d) and MB (Figure 3e) molecules on the Au-CNT-Au nanostructure is measured at spots remote from (curve 5) and near the separation area (curve 6). By depositing the molecules on the substrate and measuring Raman enhancements, we observe signature peaks at wavenumbers 434, 705, 1013, 1036, 1085, and 1585 cm^{-1} for BT (Figure 3d), and 465, 684, 786, 902, 1056, 1167, 1315, 1408, 1452, 1514, and 1636 cm^{-1} for MB, which are in correspondence with the literature.[17,20,21]

We calculate that the BT and MB analyte molecules at the separation area of the CNT forest-Au nanoparticle islands exhibit enhancement factors of 1.4×10^6 (at wavenumber 1585 cm^{-1}) and 2.3×10^6 (at wavenumber 1636 cm^{-1}), respectively. Farther from that area, the corresponding enhancement factors are calculated to be 5.8×10^5 and 1.4×10^6 (at the same wavenumbers). This means that the coupling between Au nanoparticles and CNTs increases the SERS enhancement factor nearly twice. Overall ~200% increase of Raman signal after deposition of analyte molecules on the Au-CNT-Au nanostructure is evident in Figure 3d. The presented Raman mapping results indicate coupling of CNTs to the Au nanoparticle island at the separation area, significantly increasing the effectiveness of organic molecule detection. We note that the comparatively low intensity counts in our Raman mapping experiments stemming from the short signal acquisition time (0.5 s) do not prevent us from obtaining high SERS enhancements in these measurements. The choice of using Au instead of Ag in our system is conditioned by the oxidation of the latter in air, which causes up to 3 orders of magnitude decrease of Raman signal intensity.[22]

Recently, CNT forests have been reported as potentially suitable supports for scanning near-field optical microscopy (SNOM) of Au nanoparticles deposited on top.[19] The evanescent nature of the detected waves and sub-millimetre size of the scanning tip in such experiments require a relatively flat support.[23] The strong plasmonic coupling of the Au nanoparticles to the nearby vertically-aligned nanotubes,

dx.doi.org/10.1021/am501863g | ACS Appl. Mater. Interfaces 2014, 6, 5344−5349

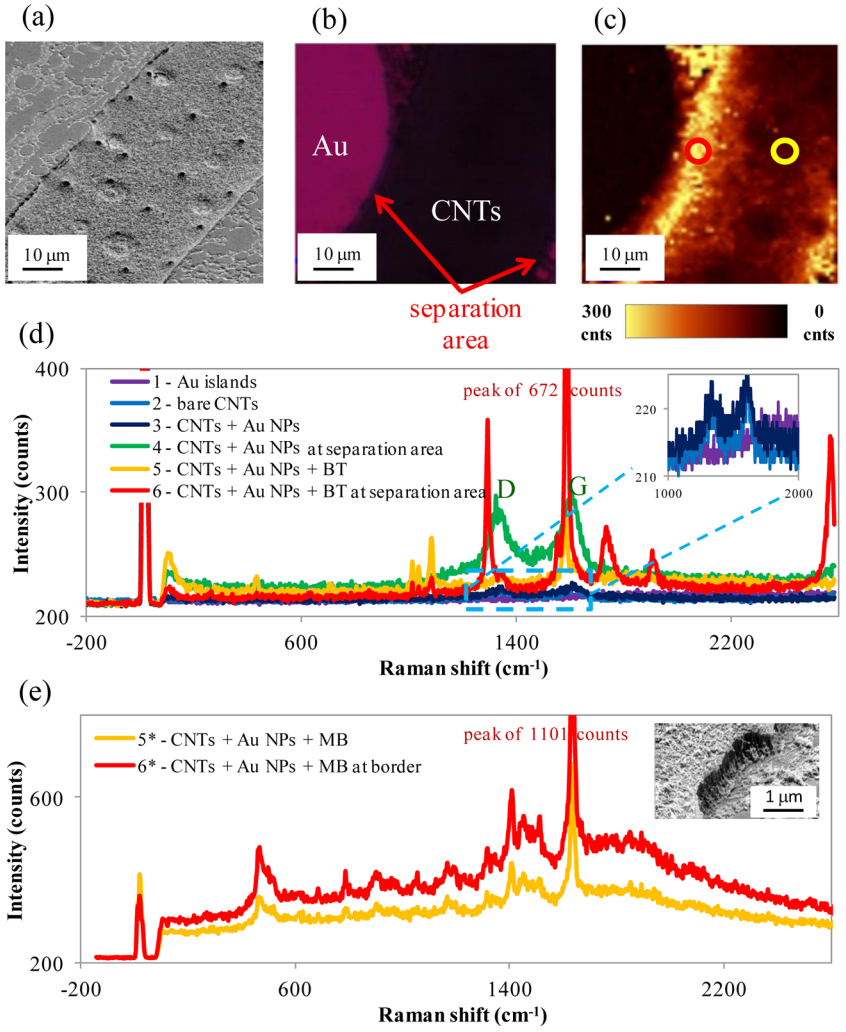

Figure 3. (a) SEM image of a typical region of CNT−Au nanoparticle hybrid after deposition of 3 nm Au, (b) an optical image of this region on which (c) Raman spectroscopic mapping is performed with a 0.25 mW 632.8 nm He−Ne laser at 0.5 s acquisition time. (d) Typical Raman spectra taken from Au nanoparticles (curve 1), CNT forests (curve 2), 3 nm Au-covered CNT forests at a spot (shown by yellow circle in c) far from the Au islands (curve 3) and at a spot (shown by red circle in c) near the border of Au islands (curve 4). The CNT D- and G- bands of curve 4 are indicated above their respective positions. Spectra of SERS measurements of the BT- (or MB-) deposited Au-CNT-Au nanostructure at spots far (curves 5 or 5*) and adjacent to (curves 6 or 6*) Au islands. Inset in d shows the zoomed Raman spectra of the curves 1−3. Inset in e shows a SEM image of the edge of the Au-CNT-Au nanostructure. The intensity is detected as counts in the coupled charge device (CCD).

demonstrated in our experiments, suggests further exploitation Au-CNT near-field optical interaction.

To verify that the Raman signal enhancement is related to SPs, we perform a series of calculations that allow corroborating our experimental results. We first calculate the SP propagation length in a dielectric substrate. We consider a binary system composed of a metal film on top of silica (dielectric) substrate. The structure is illuminated by monochromatic light source perpendicularly from below the dielectric substrate. The propagation length (distance at which the intensity drops e times) of the SPs excited on the metal−dielectric interface can thus be approximated by the following formula[24]

$$l_e = \lambda_0 \frac{(\varepsilon_m')^2}{2\pi\varepsilon_m''}\left(\frac{\varepsilon_m' + \varepsilon_d}{\varepsilon_m'\varepsilon_d}\right)^{3/2} \quad (1)$$

where ε_m' and ε_m'' are the real and imaginary parts of the metal template dielectric permittivity, ε_d is the dielectric constant of the dielectric substrate, and λ_0 is the free space wavelength of the incident light. In our Raman measurements, λ_0 = 632.8 nm. Hence, in binary systems such as Au-silica and Al_2O_3-silica, the SP propagation lengths are ∼15 and ∼1700 nm, respectively. This explains the efficient coupling between CNTs to the Au nanoparticles.

We then calculate by FEM, the influence of CNT structure on enhancement and distribution of the electric field. We simulate a system formed by a 10 nm diameter and 500 nm long nanotube separated by 3 nm from a 50 nm diamter Au nanosphere (both on a silica substrate), Figure 4. The choice of such a model system is justified by two experimental observations: (1) our CNTs are curly (because of the density of the forests) which causes negligible interaction between tubes, and (2) the SERS is strongly pronounced at the edge of Au islands and CNT forests (Figure 3c) which indicates strong coupling between the tubes and the nanoparticles. We consider two cases for the CNT permittivity: (1) semiconducting tubes (Figure 4a) and (2) metallic tubes (Figure 4b). The respective dielectric permittivity functions, taken from Butt et al.[25] and from Cui et al.[26] are plotted in Figure 4e. The dielectric permittivity of Au is taken from Johnson et al.,[27] and that of the

dx.doi.org/10.1021/am501863g | ACS Appl. Mater. Interfaces 2014, 6, 5344−5349

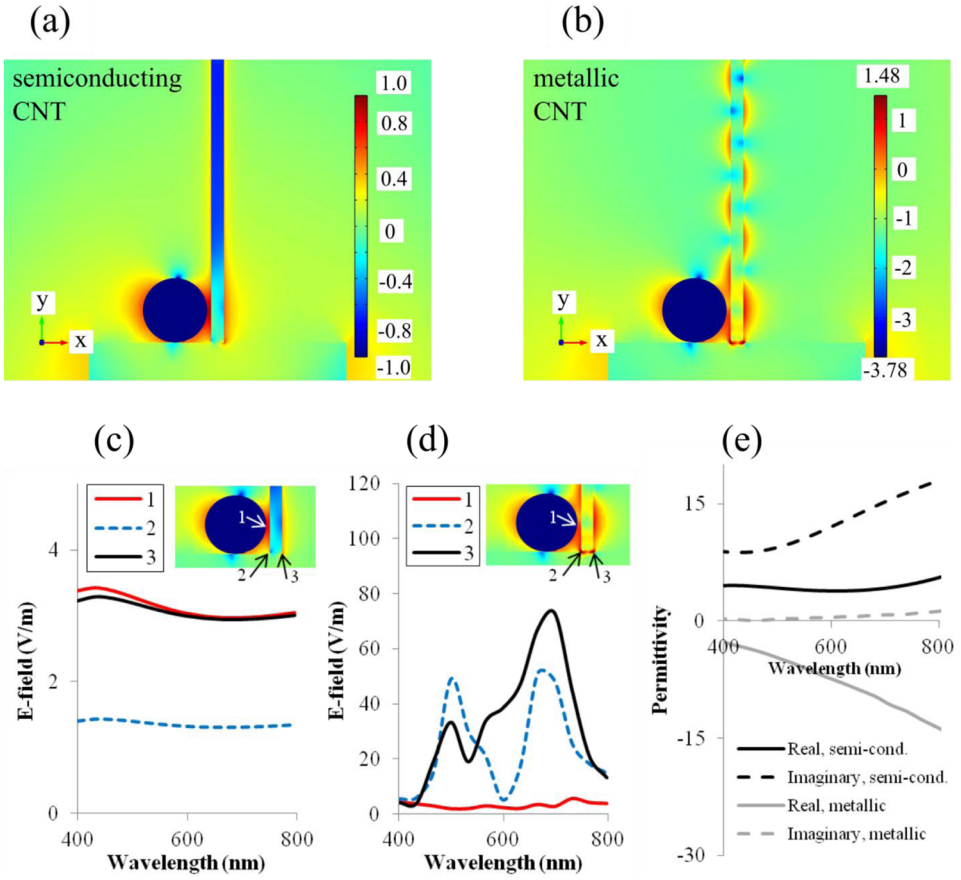

Figure 4. FEM numerical simulations on the electric field distribution and enhancement of a system of a (a) semiconducting and (b) metallic CNT of 10 nm diameter and 500 nm length standing at a 3 nm distance from a Au nanoparticle of 50 nm diameter. In a and b, the 632.8 nm wavelength incident electromagnetic wave is polarized along the *X*-axis. (c, d) Electric field enhancement at three points (the closest point of the sphere to the rod, marked by 1, and two rod edges, marked by 2 and 3) for various incident light wavelengths, for (c) semiconducting and (d) metallic CNTs, respectively. (e) Corresponding dielectric functions of the CNTs, with solid and dashed lines for real and imaginary parts, respectively.

silica substrate as 3.9. The incident out-of-plane wave is polarized parallel to the substrate.

It can be seen from panels a and b in Figure 4 that the distribution of electric field is more focused near the CNT, which is favorable for the information transfer by CNTs SP. In panels c and d in Figure 4, the electric field enhancement at three spots (pointed out in the corresponding insets) is plotted versus the incident light wavelength. These simulations reveal that metallic CNTs enhance the electromagnetic interaction of Au nanoparticles at least 30 times more than the semiconducting tubes. Moreover, Figure 4d shows that our choice of the Raman laser wavelength is justified because around this region the scattering intensity of the system is highest because of stronger coupling between the composites. Ideally, with an extended proportion of metallic-type tubes in a CNT bundle, a greater enhancement of the signal can be achieved.[28]

CONCLUSION

In conclusion, we have created a hybrid structure of CNT forests and Au nanoparticles for SERS sensing, where each of these interacting components can be used separately. The SP coupling of CNT forests to the Au nanoparticles improve the detected enhanced Raman signal involved in the near-field optical measurements by an order of magnitude. This is demonstrated by our Raman measurements as well as in FEM numerical simulations. In addition to SERS applications demonstrated on two organic molecules, this nanostructure can provide potential platforms to be employed as electrically switchable diffraction gratings in liquid crystal devices[29] as well as for more efficient energy conversion in solar cells,[30] high-resolution scanning near-field optical microscopy of noble MNPs smaller than the diffraction limiting wavelength.[31]

AUTHOR INFORMATION

Corresponding Author

*E-mail: thm34@cam.ac.ukor tmakaryan@gmail.com. Phone: +441223748317

Notes

The authors declare no competing financial interest.

ACKNOWLEDGMENTS

This work was funded in part by the European Union FP7 Project "Grafol". T.M. thanks Leo Qiang for providing a 16 Mb PC for COMSOL simulations and to Prof. Othmar Marti from Ulm University for support. M.G. thanks the "Volkswagen Stiftung" Grant 86933 for partial support.

REFERENCES

(1) De Angelis, F.; Das, G.; Candeloro, P.; Patrini, M.; Galli, M.; Bek, A.; Lazzarino, M.; Maksymov, I.; Liberale, C.; Andreani, L. C.; Di Fabrizio, E. Nanoscale Chemical Mapping Using Three-Dimensional

Adiabatic Compression of Surface Plasmon Polaritons. *Nat. Nanotechnol.* **2010**, *5* (1), 67−72.
(2) Cialla, D.; März, A.; Böhme, R.; Theil, F.; Weber, K.; Schmitt, M.; Popp, J. Surface-Enhanced Raman Spectroscopy (SERS): Progress and Trends. *Anal. Bioanal. Chem.* **2012**, *403* (1), 27−54.
(3) Kneipp, K.; Kneipp, H.; Kneipp, J. Surface-Enhanced Raman Scattering in Local Optical Fields of Silver and Gold Nanoaggregates-from Single-Molecule Raman Spectroscopy to Ultrasensitive Probing in Live Cells. *Acc. Chem. Res.* **2006**, *39* (7), 443−450.
(4) Sun, Y.; Liu, K.; Miao, J.; Wang, Z.; Tian, B.; Zhang, L.; Li, Q.; Fan, S.; Jiang, K. Highly Sensitive Surface-Enhanced Raman Scattering Substrate Made from Superaligned Carbon Nanotubes. *Nano Lett.* **2010**, *10* (5), 1747−1753.
(5) Heeg, S.; Fernandez-Garcia, R.; Oikonomou, A.; Schedin, F.; Narula, R.; Maier, S. A.; Vijayaraghavan, A.; Reich, S. Polarized Plasmonic Enhancement by Au Nanostructures Probed Through Raman Scattering of Suspended Graphene. *Nano Lett.* **2012**, *13* (1), 301−308.
(6) Wang, P.; Zhang, W.; Liang, O.; Pantoja, M.; Katzer, J.; Schroeder, T.; Xie, Y.-H. Giant Optical Response from Graphene−Plasmonic System. *ACS Nano* **2012**, *6* (7), 6244−6249.
(7) Grigorenko, A. N.; Polini, M.; Novoselov, K. S. Surface Hydrogenation and Optics of a Graphene Sheet Transferred onto a Plasmonic Nanoarray. *Nat. Photonics* **2012**, *6* (11), 749−758.
(8) Butt, H.; Dai, Q.; Farah, P.; Butler, T.; Wilkinson, T. D.; Baumberg, J. J.; Amaratunga, G. A. J. Metamaterial High Pass Filter Based on Periodic Wire Arrays of Multiwalled Carbon Nanotube. *Appl. Phys. Lett.* **2010**, *97* (16), 163102−163104.
(9) Esconjauregui, S.; Fouquet, M.; Bayer, B. C.; Ducati, C.; Smajda, R.; Hofmann, S.; Robertson, J. Growth of Ultrahigh Density Vertically Aligned Carbon Nanotube Forests For Interconnects. *ACS Nano* **2010**, *4* (12), 7431−7436.
(10) Esconjauregui, S.; Fouquet, M.; Bayer, B. C.; Eslava, S.; Khachadorian, S.; Hofmann, S.; Robertson, J. Manipulation of the Catalyst-Support Interactions for Inducing Nanotube Forest Growth. *J. Appl. Phys.* **2011**, *109* (4), 044303−044307.
(11) Prati, L.; Villa, A.; Lupini, A. R.; Veith, G. M. Gold on carbon: one billion catalysts under a single label. *Phys. Chem. Chem. Phys.* **2012**, *14* (9), 2969−2978.
(12) Lee, S.; Hahm, M. G.; Vajtai, R.; Hashim, D. P.; Thurakitseree, T.; Chipara, A. C.; Ajayan, P. M.; Hafner, J. H. Utilizing 3D SERS Active Volumes in Aligned Carbon Nanotube Scaffold Substrates. *Adv. Mater.* **2012**, *24* (38), 5261−5266.
(13) Joh, D. Y.; Kinder, J.; Herman, L. H.; Ju, S.-Y.; Segal, M. A.; Johnson, J. N.; Chan-Garnet, K. L.; Park, J. Single-Walled Carbon Nanotubes as Excitonic Optical Wires. *Nat. Nano.* **2011**, *6* (1), 51−56.
(14) Kakenov, N.; Balci, O.; Balci, S.; Kocabas, C. Single-Walled Carbon Nanotubes as Excitonic Optical Wires. *Appl. Phys. Lett.* **2012**, *101* (22), 223114−223118.
(15) Corio, P.; Brown, S. D. M.; Marucci, A.; Pimenta, M. A.; Kneipp, K.; Dresselhaus, G.; Dresselhaus, M. S. Surface-Enhanced Resonant Raman Spectroscopy of Single-Wall Carbon Nanotubes Adsorbed on Silver And Gold Surfaces. *Phys. Rev. B* **2000**, *61* (19), 13202−13211.
(16) Hartmann, N.; Piredda, G.; Berthelot, J.; Francs, G. C. D.; Bouhelier, A.; Hartschuh, A. Launching Propagating Surface Plasmon Polaritons by a Single Carbon Nanotube Dipolar Emitter. *Nano Lett.* **2012**, *12* (1), 177−181.
(17) Goldberg-Oppenheimer, P.; Hutter, T.; Chen, B.; Robertson, J.; Hofmann, S.; Mahajan, S. Optimized Vertical Carbon Nanotube Forests for Multiplex Surface-Enhanced Raman Scattering Detection. *J. Phys. Chem. Lett.* **2012**, *3* (23), 3486−3492.
(18) Dawson, P.; Duenas, J. A.; Boyle, M. G.; Doherty, M. D.; Bell, S. E. J.; Kern, A. M.; Martin, O. J. F.; Teh, A. S.; Teo, K. B. K.; Milne, W. I. Combined Antenna and Localized Plasmon Resonance in Raman Scattering from Random Arrays of Silver-Coated, Vertically Aligned Multiwalled Carbon Nanotubes. *Nano Lett.* **2011**, *11* (2), 365−371.
(19) Lu, Q.; Rao, R.; Sadanadan, B.; Que, W.; Rao, A. M.; Ke, P. C. Coupling of Photon Energy via a Multiwalled Carbon Nanotube Array. *Appl. Phys. Lett.* **2005**, *87* (17), 173102−173104.
(20) Nuntawong, N.; Horprathum, M.; Eiamchai, P.; Wong-Ek, K.; Patthanasettakul, V.; Chindaudom, P. Surface-Enhanced Raman Scattering Substrate of Silver Nanoparticles Depositing on AAO Template Fabricated by Magnetron Sputtering. *Vac.* **2010**, *84* (12), 1415−1418.
(21) Harpster, M. H.; Zhang, H.; Sankara-Warrier, A. K.; Ray, B. H.; Ward, T. R.; Kollmar, J. P.; Carron, K. T.; Mecham, J. O.; Corcoran, R. C.; Wilson, W. C.; Johnson, P. A. SERS Detection of Indirect Viral DNA Capture Using Colloidal Gold and Methylene Blue as a Raman Label. *Biosens. Bioelectron.* **2009**, *25* (4), 674−681.
(22) Han, Y.; Lupitskyy, R.; Chou, T.-M.; Stafford, C. M.; Du, H.; Sukhishvili, S. Effect of Oxidation on Surface-Enhanced Raman Scattering Activity of Silver Nanoparticles: a Quantitative Correlation. *Anal. Chem.* **2011**, *83* (15), 5873−5880.
(23) Mihaljevic, J.; Hafner, C.; Meixner, A. J. Simulation of a Metallic SNOM Tip Illuminated by a Parabolic Mirror. *Opt. Expr.* **2013**, *21* (22), 25926−25943.
(24) Barnes, W. L. Surface Plasmon−Polariton Length Scales: a Route to Sub-Wavelength Optics. *J. Opt. A: Pure Appl. Opt.* **2006**, *8* (4), S87−S93.
(25) Butt, H.; Butler, T.; Montelongo, Y.; Rajesekharan, R.; Wilkinson, T. D.; Amaratunga, G. A. Continuous Diffraction Patterns from Circular Arrays of Carbon Nanotubes J. *Appl. Phys. Lett.* **2012**, *101* (25), 251102−2511024.
(26) Cui, X.; Dong, L.; Zhang, W.; Wu, W.; Tang, Y.; Erni, D. Numerical Investigations of a Multi-Walled Carbon Nanotube-Based Multi-Segmented Optical Antenna. *Appl. Phys. B* **2010**, *101* (3), 601−609.
(27) Johnson, P. B.; Christy, R. W. Optical Constants of the Noble Metals. *Phys. Rev. B* **1972**, *6* (12), 4370−4379.
(28) Shuba, M. V.; Paddubskaya, A. G.; Plyushch, A. O.; Kuzhir, P. P.; Slepyan, G. Y.; Maksimenko, S. A.; Ksenevich, V. K.; Buka, P.; Seliuta, D.; Kasalynas, I.; Macutkevic, J.; Valusis, G.; Thomsen, C.; Lakhtakia, A. Experimental Evidence of Localized Plasmon Resonance in Composite Materials Containing Single-Wall Carbon Nanotubes. *Phys. Rev. B* **2012**, *85* (16), 165435−165440.
(29) Won, K.; Palani, A.; Butt, H.; Hands, P. J. W.; Rajeskharan, R.; Dai, Q.; Khan, A. A.; Amaratunga, G. A. J.; Coles, H. J.; Wilkinson, T. D. Electrically Switchable Diffraction Grating Using a Hybrid Liquid Crystal and Carbon Nanotube-Based Nanophotonic Device. *Adv. Opt. Mater.* **2013**, *1*, 368−373.
(30) Li, Y.; Kodama, S.; Kaneko, T.; Hatakeyama, R. Performance Enhancement of Solar Cells Based on Single-Walled Carbon Nanotubes by Au Nanoparticles. *Appl. Phys. Lett.* **2012**, *101*, 083901−083904.
(31) Mahjouri-Samani, M.; Zhou, Y. S.; He, X. N.; Xiong, W.; Hilger, P.; Lu, Y. F. Plasmonic-Enhanced Carbon Nanotube Infrared Bolometers. *Nanotechnology* **2013**, *24*, 035502−035508.